

X-Dreamer: Creating High-quality 3D Content by Bridging the Domain Gap Between Text-to-2D and Text-to-3D Generation

Yiwei Ma^{1‡} Yijun Fan^{1‡} Jiayi Ji¹ Haowei Wang¹
 Xiaoshuai Sun^{1*} Guannan Jiang² Annan Shu² Rongrong Ji¹

¹Key Laboratory of Multimedia Trusted Perception and Efficient Computing, Ministry of Education of China, Xiamen University, 361005, P.R. China.

²Contemporary Ampere Technology Co., Limited (CATL), Fujian, China

Abstract

In recent times, automatic text-to-3D content creation has made significant progress, driven by the development of pretrained 2D diffusion models. Existing text-to-3D methods typically optimize the 3D representation to ensure that the rendered image aligns well with the given text, as evaluated by the pretrained 2D diffusion model. Nevertheless, a substantial domain gap exists between 2D images and 3D assets, primarily attributed to variations in camera-related attributes and the exclusive presence of foreground objects. Consequently, employing 2D diffusion models directly for optimizing 3D representations may lead to suboptimal outcomes. To address this issue, we present X-Dreamer, a novel approach for high-quality text-to-3D content creation that effectively bridges the gap between text-to-2D and text-to-3D synthesis. The key components of X-Dreamer are two innovative designs: Camera-Guided Low-Rank Adaptation (CG-LoRA) and Attention-Mask Alignment (AMA) Loss. CG-LoRA dynamically incorporates camera information into the pretrained diffusion models by employing camera-dependent generation for trainable parameters. This integration enhances the alignment between the generated 3D assets and the camera’s perspective. AMA loss guides the attention map of the pretrained diffusion model using the binary mask of the 3D object, prioritizing the creation of the foreground object. This module ensures that the model focuses on generating accurate and detailed foreground objects. Extensive evaluations demonstrate the effectiveness of our proposed method compared to existing text-to-3D approaches. Our project webpage: <https://xmu-xiaoma666.github.io/Projects/X-Dreamer>.

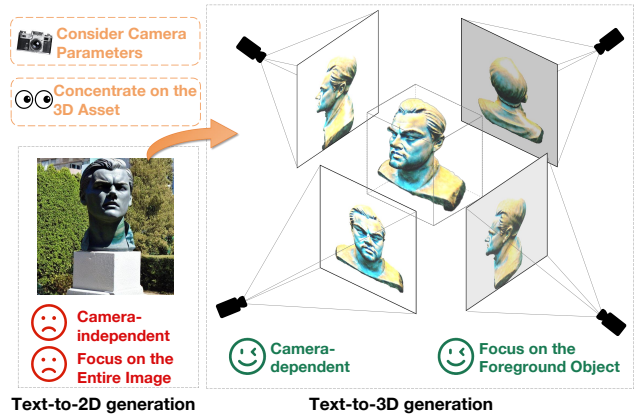


Figure 1. The outputs of the text-to-2D generation model (left) and the text-to-3D generation model (right) under the same text prompt, i.e., “A statue of Leonardo DiCaprio’s head”.

1. Introduction

The field of text-to-3D synthesis, which seeks to generate superior 3D content predicated on input textual descriptions, has shown significant potential to impact a diverse range of applications. These applications extend beyond traditional areas such as architecture, animation, and gaming, and encompass contemporary domains like virtual and augmented reality.

In recent years, extensive research has demonstrated significant performance improvement in the text-to-2D generation task [2, 24–26] by leveraging pretrained diffusion models [6, 30, 31] on a large-scale text-image dataset [27]. Building on these advancements, DreamFusion [22] introduces an effective approach that utilizes a pretrained 2D diffusion model [26] to autonomously generate 3D assets from text, eliminating the need for a dedicated 3D asset dataset. A key innovation introduced by DreamFusion is the Score Distillation Sampling (SDS) algorithm. This algorithm aims to optimize a single 3D representation, such as

*Corresponding author; ‡Equal contributions.

NeRF [18], to ensure that rendered images from any camera perspective maintain a high likelihood with the given text, as evaluated by the pretrained 2D diffusion model. Inspired by the groundbreaking SDS algorithm, several recent works [4, 13, 16, 35, 36] have emerged, envisioning the text-to-3D generation task through the application of pretrained 2D diffusion models.

While text-to-3D generation has made significant strides through the utilization of pretrained text-to-2D diffusion models, it is crucial to recognize and address the persistent and substantial domain gap that remains between text-to-2D and text-to-3D generation. This distinction is clearly illustrated in Fig. 1. To begin with, the text-to-2D model produces camera-independent generation results, focusing on generating high-quality images from specific angles while disregarding other angles. In contrast, 3D content creation is intricately tied to camera parameters such as position, shooting angle, and field of view. As a result, a text-to-3D model must generate high-quality results across all possible camera parameters. This fundamental difference emphasizes the necessity for innovative approaches that enable the pretrained diffusion model to consider camera parameters. Furthermore, a text-to-2D generation model must simultaneously generate both foreground and background elements while maintaining the overall coherence of the image. Conversely, a text-to-3D generation model only needs to concentrate on creating the foreground object. This distinction allows text-to-3D models to allocate more resources and attention to precisely represent and generate the foreground object. Consequently, the domain gap between text-to-2D and text-to-3D generation poses a significant performance obstacle when directly employing pretrained 2D diffusion models for 3D asset creation.

In this study, we present a pioneering framework, X-Dreamer, designed to address the domain gap between text-to-2D and text-to-3D generation, thereby facilitating the creation of high-quality text-to-3D content. Our framework incorporates two innovative designs that are specifically tailored to address the aforementioned challenges. Firstly, existing approaches [4, 13, 16, 35] commonly employ 2D pretrained diffusion models [25, 26] for text-to-3D generation, which lack inherent linkage to camera parameters. To address this limitation and ensure that our text-to-3D model produces results that are directly influenced by camera parameters, we introduce *Camera-Guided Low-Rank Adaptation (CG-LoRA)* to fine-tune the pretrained 2D diffusion model. Notably, the parameters of CG-LoRA are dynamically generated based on the camera information during each iteration, establishing a robust relationship between the text-to-3D model and camera parameters. Furthermore, pretrained text-to-2D diffusion models allocate attention to both foreground and background generation, whereas the creation of 3D assets necessitates a stronger focus on ac-

curately generating foreground objects. To address this requirement, we introduce *Attention-Mask Alignment (AMA) Loss*, which leverages the rendered binary mask of the 3D object to guide the attention map of the pretrained 2D stable diffusion model [25]. By incorporating this module, X-Dreamer prioritizes the generation of foreground objects, resulting in a significant enhancement of the overall quality of the generated 3D content.

We present a compelling demonstration of the effectiveness of X-Dreamer in synthesizing high-quality 3D assets based on textual cues. By incorporating CG-LoRA and AMA loss to address the domain gap between text-to-2D and text-to-3D generation, our proposed framework exhibits substantial advancements over prior methods in text-to-3D generation. In summary, our study contributes to the field in three key aspects:

- We propose a novel method, X-Dreamer, for high-quality text-to-3D content creation, effectively bridging the domain gap between text-to-2D and text-to-3D generation.
- To enhance the alignment between the generated results and the camera perspective, we propose CG-LoRA, which leverages camera information to dynamically generate specific parameters for 2D diffusion models.
- To prioritize the creation of foreground objects in the text-to-3D model, we introduce AMA loss, which utilizes binary masks of the foreground 3D object to guide the attention maps of the 2D diffusion model.

2. Related Work

2.1. Text-to-3D Content Creation

In recent years, there has been a significant surge in interest surrounding the evolution of text-to-3D generation [12, 17, 22]. This growing field has been propelled, in part, by advancements in pretrained vision-and-language models, such as CLIP [23], as well as diffusion models like Stable Diffusion [25] and Imagen [26]. Contemporary text-to-3D models can generally be classified into two distinct categories: *the CLIP-based text-to-3D approach* and *the diffusion-based text-to-3D approach*. The CLIP-based text-to-3D approach [9, 11, 14, 17, 19, 37] employs CLIP encoders [23] to project textual descriptions and rendered images derived from the 3D object into a modal-shared feature space. Subsequently, CLIP loss is harnessed to align features from both modalities, optimizing the 3D representation to conform to the textual description. Various scholars have made significant contributions to this field. For instance, Michel *et al.* [17] are pioneers in proposing the use of CLIP loss to harmonize the text prompt with the rendered images of the 3D object, thereby enhancing text-to-3D generation. Ma *et al.* [14] introduce dynamic textual guidance during 3D object synthesis to improve convergence speed and generation performance. However, these approaches

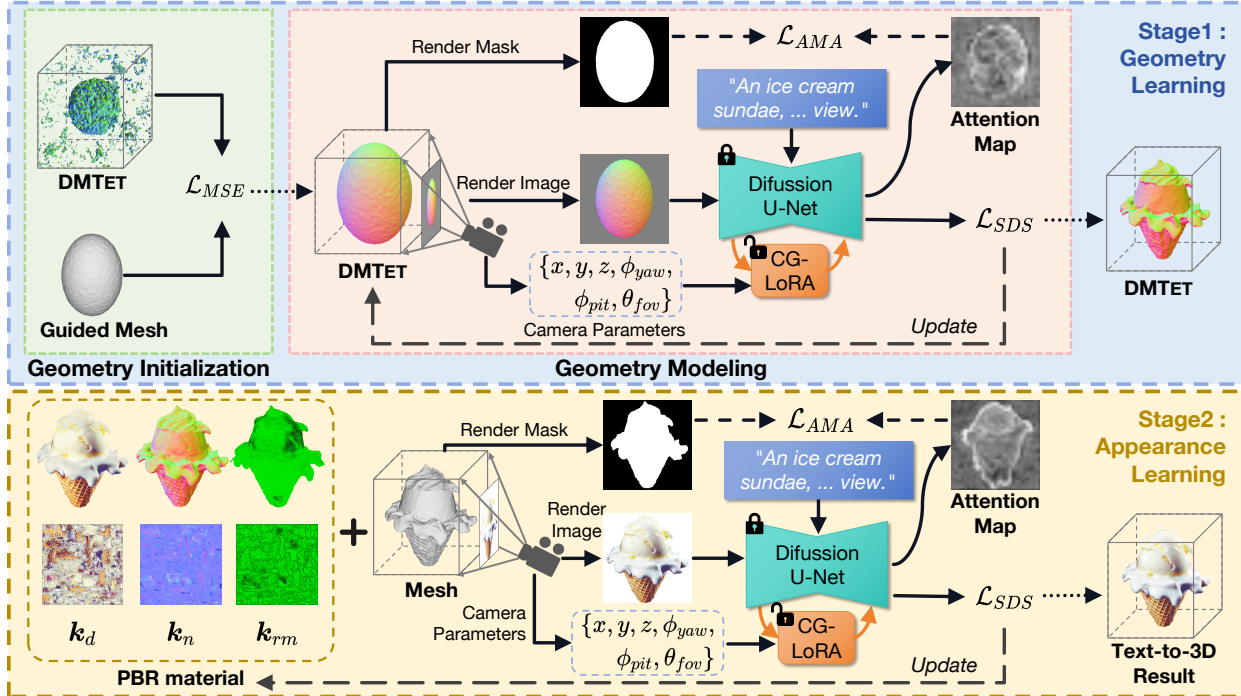


Figure 2. Overview of the proposed X-Dreamer, which consists of geometry learning and appearance learning.

have inherent limitations, as they tend to generate 3D representations with a scarcity of geometry and appearance detail. To overcome this shortcoming, the diffusion-based text-to-3D approach [4, 8, 10, 13, 22, 32] leverages pre-trained text-to-2D diffusion models [25, 26] to guide the optimization of 3D representations. Central to these models is the application of SDS loss [22] to align the rendered images stemming from a variety of camera perspectives with the textual description. Specifically, given the target text prompt, Lin *et al.* [13] leverage a coarse-to-fine pipeline to generate high-resolution 3D content. Chen *et al.* [4] decouple geometry modeling and appearance modeling to generate realistic 3D assets. For specific purposes, some researchers [28, 36] integrate trainable LoRA [7] branches into pre-trained diffusion models. For instance, Seo *et al.* [28] put forth 3DFuse, a model that harnesses the power of LoRA to comprehend object semantics. Wang *et al.* [36] introduce ProlificDreamer, where the role of LoRA is to evaluate the score of the variational distribution for 3D parameters. However, the LoRA parameter begins its journey from random initialization and maintains its independence from the camera and text. To address these limitations, we present two innovative modules: CG-LoRA and AMA loss. These modules are designed to enhance the model’s ability to consider important camera parameters and prioritize the generation of foreground objects throughout the text-to-3D creation process.

2.2. Low-Rank Adaptation (LoRA)

Low-Rank Adaptation (LoRA) is a technique used to reduce memory requirements when fine-tuning a large model. It involves injecting only a small set of trainable parameters into the pre-trained model, while keeping the original parameters fixed. During the optimization process, gradients are passed through the fixed pre-trained model weights to the LoRA adapter, which is then updated to optimize the loss function. LoRA has been applied in various fields, including natural language processing [3, 7], image synthesis [38] and 3D generation [28, 36]. To achieve low-rank adaptation, a linear projection with a pre-trained weight matrix $\mathbf{W}_0 \in \mathbb{R}^{d_{in} \times d_{out}}$ is augmented with an additional low-rank factorized projection. This augmentation is represented as $\mathbf{W}_0 + \Delta\mathbf{W} = \mathbf{W}_0 + \mathbf{A}\mathbf{B}$, where $\mathbf{A} \in \mathbb{R}^{d_{in} \times r}$, $\mathbf{B} \in \mathbb{R}^{r \times d_{out}}$, and $r \ll \min(d_{in}, d_{out})$. During training, \mathbf{W}_0 remains fixed, while \mathbf{A} and \mathbf{B} are trainable. The modified forward pass, given the original forward pass $\mathbf{Y} = \mathbf{X}\mathbf{W}_0$, can be formulated as follows:

$$\mathbf{Y} = \mathbf{X}\mathbf{W}_0 + \mathbf{X}\mathbf{A}\mathbf{B}. \quad (1)$$

In this paper, we introduce CG-LoRA, which involves the dynamic generation of trainable parameters for \mathbf{A} based on camera information. This technique allows for integrating perspective information, including camera parameters and direction-aware descriptions, into the pre-trained text-to-2D diffusion model. As a result, our method significantly enhances text-to-3D generation capabilities.

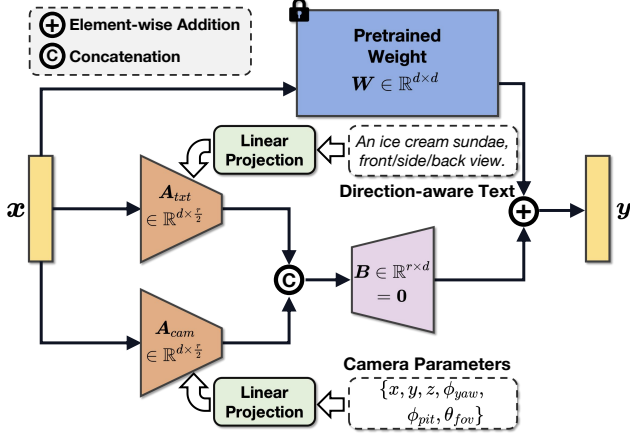


Figure 3. Illustration of Camera-Guided Low-Rank Adaptation.

3. Approach

3.1. Architecture

In this section, we present a comprehensive introduction to the proposed X-Dreamer, which consists of two main stages: geometry learning and appearance learning. For geometry learning, we employ DMTET [29] as the 3D representation. DMTET is an MLP parameterized with Φ_{dmt} and is initialized with a 3D ellipsoid using the mean squared error (MSE) loss \mathcal{L}_{MSE} . Subsequently, we optimize DMTET and CG-LoRA using the SDS loss [22] \mathcal{L}_{SDS} and the proposed AMA loss \mathcal{L}_{AMA} to ensure the alignment between the 3D representation and the input text prompt. For appearance learning, we leverage bidirectional reflectance distribution function (BRDF) modeling [33] following the previous approach [4]. Specifically, we utilize an MLP with trainable parameters Φ_{mat} to predict surface materials. Similar to the geometry learning stage, we optimize Φ_{mat} and CG-LoRA using the SDS loss \mathcal{L}_{SDS} and the AMA loss \mathcal{L}_{AMA} to achieve alignment between the 3D representation and the text prompt. Fig. 2 provides a detailed depiction of our proposed X-Dreamer.

Geometry Learning. For geometry learning, an MLP network Φ_{dmt} is utilized to parameterize DMTET as a 3D representation. To enhance the stability of geometry modeling, we employ a 3D ellipsoid as the initial configuration for DMTET Φ_{dmt} . For each vertex $v_i \in V_T$ belonging to the tetrahedral grid T , we train Φ_{dmt} to predict two important values: the SDF value $s(v_i)$ and the deformation offset $\delta(v_i)$. To initialize Φ_{dmt} with the 3D ellipsoid, we sample a set of N points $\{p_i \in \mathbb{R}^3\}_{i=1}^N$ approximately distributed on the surface of an ellipsoid and compute the corresponding SDF values $\{SDF(p_i)\}_{i=1}^N$. Subsequently, we optimize Φ_{dmt} using MSE loss. This optimization process ensures that Φ_{dmt} effectively initializes DMTET to resemble the 3D

ellipsoid. The formulation of the MSE loss is given by:

$$\mathcal{L}_{MSE} = \frac{1}{N} \sum_{i=1}^N (s(p_i; \Phi_{dmt}) - SDF(p_i))^2. \quad (2)$$

After initializing the geometry, our objective is to align the geometry of DMTET with the input text prompt. Specifically, we generate the normal map \mathbf{n} and the object mask \mathbf{m} from the initialized DMTET Φ_{dmt} by employing a differentiable rendering technique [33], given a randomly sampled camera pose \mathbf{c} . Subsequently, we input the normal map \mathbf{n} into the frozen stable diffusion (SD) with a trainable CG-LoRA and update Φ_{dmt} using the SDS loss, which is defined as follows:

$$\nabla_{\Phi_{dmt}} \mathcal{L}_{SDS} = \mathbb{E}_{t, \epsilon} \left[w(t) (\hat{\epsilon}_{\Theta}(\mathbf{n}_t; \mathbf{y}, t) - \epsilon) \frac{\partial \mathbf{n}}{\partial \Phi_{dmt}} \right], \quad (3)$$

where Θ represents the parameter of SD, $\hat{\epsilon}_{\Theta}(\mathbf{n}_t; \mathbf{y}, t)$ denotes the predicted noise of SD given the noise level t and text embedding \mathbf{y} . Additionally, $\mathbf{n}_t = \alpha_t \mathbf{n} + \sigma_t \epsilon$, where $\epsilon \sim \mathcal{N}(\mathbf{0}, \mathbf{I})$ represents noise sampled from a normal distribution. The implementation of $w(t)$, α_t , and σ_t is based on the DreamFusion [22].

Furthermore, to focus SD on generating foreground objects, we introduce an additional AMA loss to align the object mask \mathbf{m} with the attention map of SD, given by:

$$\mathcal{L}_{AMA} = \frac{1}{L} \sum_{i=1}^L |\mathbf{a}_i - \eta(\mathbf{m})|, \quad (4)$$

where L denotes the number of attention layers, and \mathbf{a}_i is the attention map of i -th attention layer. The function $\eta(\cdot)$ is employed to resize the rendered mask, ensuring its dimensions align with those of the attention maps.

Appearance Learning. After obtaining the geometry of the 3D object, our objective is to compute its appearance using the Physically-Based Rendering (PBR) material model [15]. The material model comprises the diffuse term $\mathbf{k}_d \in \mathbb{R}^3$, the roughness and metallic term $\mathbf{k}_{rm} \in \mathbb{R}^2$, and the normal variation term $\mathbf{k}_n \in \mathbb{R}^3$. For any point $p \in \mathbb{R}^3$ on the surface of the geometry, we utilize an MLP parameterized by Φ_{mat} to obtain the three material terms, which can be expressed as follows:

$$(\mathbf{k}_d, \mathbf{k}_n, \mathbf{k}_{rm}) = \text{MLP}(\mathcal{P}(p); \Phi_{mat}), \quad (5)$$

where $\mathcal{P}(\cdot)$ represents the positional encoding using a hash-grid technique [20]. Subsequently, each pixel of the rendered image can be computed as follows:

$$V(p, \omega) = \int_{\Omega} L_i(p, \omega_i) f(p, \omega_i, \omega) (\omega_i \cdot \mathbf{n}_p) d\omega_i, \quad (6)$$

where $V(p, \omega)$ denotes the rendered pixel value from the direction ω for the surface point p . Ω denotes a hemisphere

defined by the set of incident directions ω_i satisfying the condition $\omega_i \cdot n_p \geq 0$, where ω_i denotes the incident direction, and n_p represents the surface normal at point p . $L_i(\cdot)$ corresponds to the incident light from an off-the-shelf environment map, and $f(\cdot)$ is the Bidirectional Reflectance Distribution Function (BRDF) related to the material properties (*i.e.*, $\mathbf{k}_d, \mathbf{k}_n, \mathbf{k}_{rm}$). By aggregating all rendered pixel colors, we obtain a rendered image $\mathbf{x} = \{V(p, \omega)\}$. Similar to the geometry modeling stage, we feed the rendered image \mathbf{x} into SD. The optimization objective remains the same as Eq. (3) and Eq. (4), where the rendered normal map \mathbf{n} and the parameters of DMTET Φ_{det} are replaced with the rendered image \mathbf{x} and the parameters of the material encoder Φ_{mat} , respectively.

3.2. Camera-Guided Low-Rank Adaptation

The domain gap between text-to-2D and text-to-3D generation presents a significant challenge, as discussed in Sec. 1. It has been observed that directly utilizing pretrained SD for text-to-3D generation can result in certain issues, such as the Janus Problem [1, 12]. To address these issues, we propose Camera-Guided Low-Rank Adaptation (CG-LoRA) as a solution to bridge the domain gap. As depicted in Fig. 20, we leverage camera parameters and direction-aware text to guide the generation of parameters in CG-LoRA, enabling X-Dreamer to effectively incorporate camera perspective and direction information.

Specifically, given a text prompt T and camera parameters $C = \{x, y, z, \phi_{yaw}, \phi_{pit}, \theta_{fov}\}$ ¹, we initially project these inputs into a feature space using the pretrained textual CLIP encoder $\mathcal{E}_{txt}(\cdot)$ and a trainable MLP $\mathcal{E}_{pos}(\cdot)$:

$$\mathbf{t} = \mathcal{E}_{txt}(T), \quad (7)$$

$$\mathbf{c} = \mathcal{E}_{pos}(C), \quad (8)$$

where $\mathbf{t} \in \mathbb{R}^{d_{txt}}$ and $\mathbf{c} \in \mathbb{R}^{d_{cam}}$ are textual features and camera features. Subsequently, we employ two low-rank matrices to project \mathbf{t} and \mathbf{c} into trainable dimensionality-reduction matrices within CG-LoRA:

$$\mathbf{A}_{txt} = \text{Reshape}(\mathbf{t}\mathbf{W}_{txt}), \quad (9)$$

$$\mathbf{A}_{cam} = \text{Reshape}(\mathbf{c}\mathbf{W}_{cam}), \quad (10)$$

where $\mathbf{A}_{txt} \in \mathbb{R}^{d \times \frac{r}{2}}$ and $\mathbf{A}_{cam} \in \mathbb{R}^{d \times \frac{r}{2}}$ are two dimensionality-reduction matrices of CG-LoRA. The function $\text{Reshape}(\cdot)$ is used to transform the shape of a tensor from $\mathbb{R}^{d \times \frac{r}{2}}$ to $\mathbb{R}^{d \times \frac{r}{2}}$.² $\mathbf{W}_{txt} \in \mathbb{R}^{d_{txt} \times (d \times \frac{r}{2})}$ and $\mathbf{W}_{cam} \in \mathbb{R}^{d_{cam} \times (d \times \frac{r}{2})}$ are two low-rank matrices. Thus,

¹The variables $x, y, z, \phi_{yaw}, \phi_{pit}, \theta_{fov}$ represent the x, y, z coordinates, yaw angle, pitch angle of the camera, and field of view, respectively. The roll angle ϕ_{roll} is intentionally set to 0 to ensure the stability of the object in the rendered image.

² $\mathbb{R}^{d \times \frac{r}{2}}$ denotes a one-dimensional vector. $\mathbb{R}^{d \times \frac{r}{2}}$ represents a two-dimensional matrix.

we decompose them into the product of two matrices to reduce the trainable parameters in our implementation, *i.e.*, $\mathbf{W}_{txt} = \mathbf{U}_{txt}\mathbf{V}_{txt}$ and $\mathbf{W}_{cam} = \mathbf{U}_{cam}\mathbf{V}_{cam}$, where $\mathbf{U}_{txt} \in \mathbb{R}^{d_{txt} \times r'}$, $\mathbf{V}_{txt} \in \mathbb{R}^{r' \times (d \times \frac{r}{2})}$, $\mathbf{U}_{cam} \in \mathbb{R}^{d_{cam} \times r'}$, $\mathbf{V}_{cam} \in \mathbb{R}^{r' \times (d \times \frac{r}{2})}$, r' is a small number (*i.e.*, 4). In accordance with LoRA [7], we initialize the dimensionality-expansion matrix $\mathbf{B} \in \mathbb{R}^{r \times d}$ with zero values to ensure that the model begins training from the pretrained parameters of SD. Thus, the feed-forward process of CG-LoRA is formulated as follows:

$$\mathbf{y} = \mathbf{x}\mathbf{W} + [\mathbf{x}\mathbf{A}_{txt}; \mathbf{x}\mathbf{A}_{cam}]\mathbf{B}, \quad (11)$$

where $\mathbf{W} \in \mathbb{R}^{d \times d}$ represents the frozen parameters of the pretrained SD model, and $[\cdot; \cdot]$ is the concatenation operation along the channel dimension. In our implementation, we integrate CG-LoRA into the linear embedding layers of the attention modules in SD to effectively capture direction and camera information.

3.3. Attention-Mask Alignment Loss

Although SD is pretrained to generate 2D images that encompass both foreground and background elements, the task of text-to-3D generation demands a stronger focus on generating foreground objects. To address this specific requirement, we introduce Attention-Mask Alignment (AMA) Loss, which aims to align the attention map of SD with the rendered mask image of the 3D object. Specifically, for each attention layer in the pretrained SD, we compute the attention map between the query image feature $\mathbf{Q} \in \mathbb{R}^{H \times h \times w \times \frac{d}{H}}$ and the key CLS token feature $\mathbf{K} \in \mathbb{R}^{H \times \frac{d}{H}}$. The calculation is formulated as follows:

$$\bar{\mathbf{a}} = \text{Softmax}\left(\frac{\mathbf{Q}\mathbf{K}^\top}{\sqrt{d}}\right), \quad (12)$$

where H denotes the number of attention heads in SD, and $\bar{\mathbf{a}} \in \mathbb{R}^{H \times h \times w}$ represents the attention map. Subsequently, we proceed to compute the overall attention map $\hat{\mathbf{a}} \in \mathbb{R}^{h \times w}$ by averaging the attention values of $\bar{\mathbf{a}}$ across all attention heads. Since the attention map values are normalized using the softmax function, the activation values in the attention map may become very small when the image feature resolution is high. However, considering that each element in the rendered mask has a binary value of either 0 or 1, directly aligning the attention map with the rendered mask is not optimal. To address this, we propose a normalization technique that maps the values in the attention map from 0 to 1. This normalization process is formulated as follows:

$$\mathbf{a} = \frac{\hat{\mathbf{a}} - \min(\hat{\mathbf{a}})}{\max(\hat{\mathbf{a}}) - \min(\hat{\mathbf{a}}) + \nu}, \quad (13)$$

where ν represents a small constant value (*e.g.*, $1e-6$) that prevents division by zero in the denominator. Finally, we

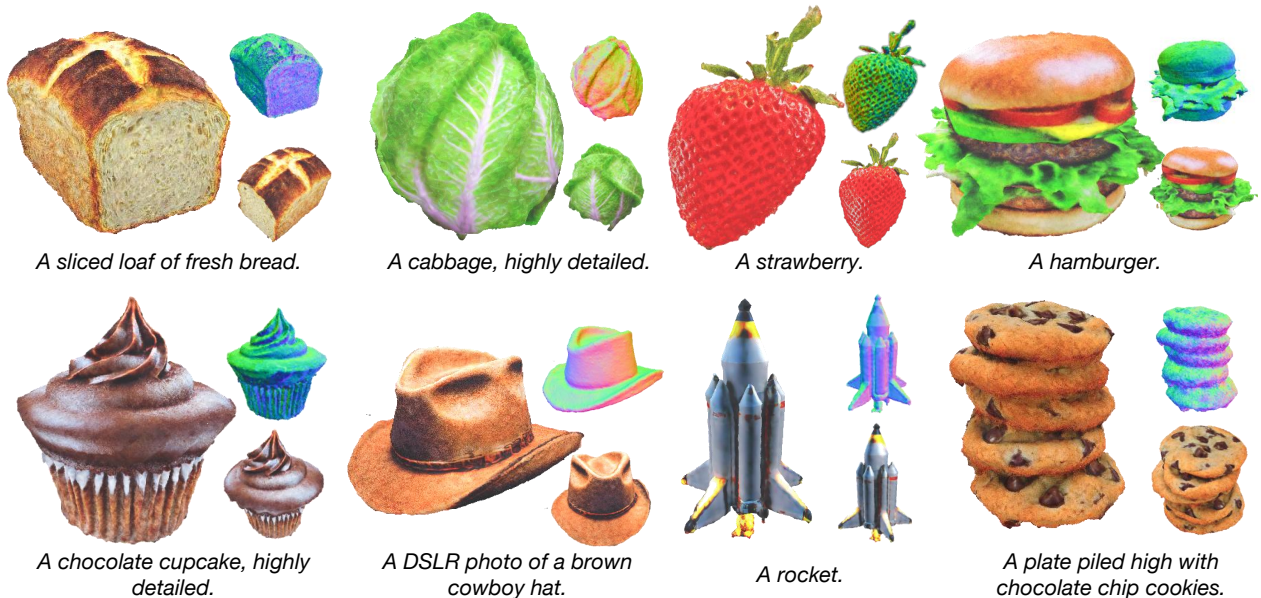


Figure 4. Text-to-3D generation results from an ellipsoid.



Figure 5. Text-to-3D generation results from coarse-grained guided meshes.

align the attention maps of all attention layers with the rendered mask of the 3D object using the AMA loss. The formulation of this alignment is presented in Eq. (4).

4. Experiments

4.1. Implementation Details.

We conduct the experiments using four Nvidia RTX 3090 GPUs and the PyTorch library [21]. To calculate the SDS loss, we utilize the Stable Diffusion implemented by HuggingFace Diffusers [34]. For the DMTET Φ_{dmt} and material encoder Φ_{mat} , we implement them as a two-layer MLP and a single-layer MLP, respectively, with a hidden dimension of 32. The values of d_{cam} , d_{txt} , r , r' , the batch size, the SDS loss weight, the AMA loss weight, and the aspect ratio of the perspective projection plane are set to 1024, 1024, 4, 4, 4, 1, 0.1, and 1 respectively. We optimize X-Dreamer for 2000 iterations for geometry learning and 1000

iterations for appearance learning. For each iteration, ϕ_{pit} , ϕ_{yaw} , and θ_{fov} are randomly sampled from $(-15^\circ, 45^\circ)$, $(-180^\circ, 180^\circ)$, and $(25^\circ, 45^\circ)$, respectively.

4.2. Results of X-Dreamer

Text-to-3D generation from an ellipsoid. We present representative results of X-Dreamer for text-to-3D generation, utilizing an ellipsoid as the initial geometry, as shown in Fig. 4. The results demonstrate the ability of X-Dreamer to generate high-quality and photo-realistic outputs that accurately correspond to the input text prompts.

Text-to-3D generation from coarse-grained meshes. While there is a wide availability of coarse-grained meshes for download from the internet, directly utilizing these meshes for 3D content creation often results in poor performance due to the lack of geometric details. However, when compared to a 3D ellipsoid, these meshes may provide better 3D shape prior information for X-Dreamer. Hence, in-

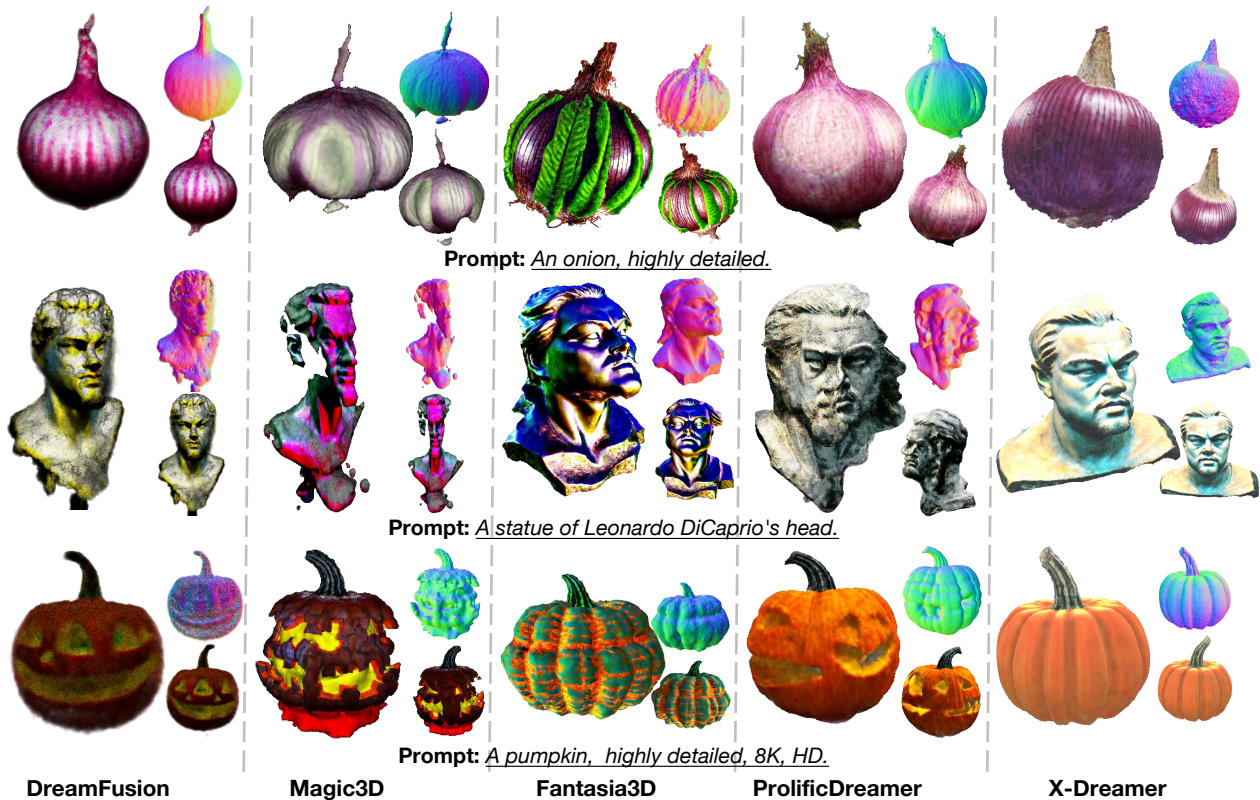


Figure 6. Comparison with State-of-the-Art (SOTA) methods. Our method yields results that exhibit enhanced fidelity and more details.

stead of using ellipsoids, we can initialize DMTET with coarse-grained guided meshes as well. As shown in Fig. 5, X-Dreamer can generate 3D assets with precise geometric details based on the given text, even when the provided coarse-grained mesh lacks details. For instance, in the last column of Fig. 5, X-Dreamer accurately transforms the geometry from a cow to a corgi based on the text prompt “A corgi, highly detailed.” Therefore, X-Dreamer is also an exceptionally powerful tool for editing coarse-grained mesh geometry using textual inputs.

Qualitative Comparison. To assess the effectiveness of X-Dreamer, we compare it with four SOTA methods: DreamFusion [22], Magic3D [13], Fantasia3D [4], and ProlificDreamer [36], as depicted in Fig. 6. When compared to the SDS-based methods [13, 22, 36], X-Dreamer outperforms them in generating superior-quality and realistic 3D assets. In addition, when compared to the VSD-based method [36], X-Dreamer produces 3D content with comparable or even better visual effects, while requiring significantly less optimization time. Specifically, the geometry and appearance learning process of X-Dreamer requires only approximately 27 minutes, whereas ProlificDreamer exceeds 8 hours.

4.3. Ablation Study

Ablation on the proposed modules. To gain insights into the abilities of CG-LoRA and AMA loss, we perform ablation studies wherein each module is incorporated individually to assess its impact. As depicted in Fig. 7, the ablation

results demonstrate a notable decline in the geometry and appearance quality of the generated 3D objects when CG-LoRA is excluded from X-Dreamer. For instance, as shown in the second row of Fig. 7, the generated Batman lacks an ear on the top of its head in the absence of CG-LoRA. This observation highlights the crucial role of CG-LoRA in injecting camera-relevant information into the model, thereby enhancing the 3D consistency. Furthermore, the omission of AMA loss from X-Dreamer also has a deleterious effect on the geometry and appearance fidelity of the generated 3D assets. Specifically, as illustrated in the first row of Fig. 7, X-Dreamer successfully generates a photorealistic texture for the rocket, whereas the texture quality noticeably deteriorates in the absence of AMA loss. This disparity can be attributed to AMA loss, which directs the focus of the model towards foreground object generation, ensuring the realistic representation of both geometry and appearance of foreground objects. These ablation studies provide valuable insights into the individual contributions of CG-LoRA and AMA loss in enhancing the geometry, appearance, and overall quality of the generated 3D objects.

Attention map comparisons w/ and w/o AMA loss. AMA loss is introduced with the aim of guiding attention during the denoising process towards the foreground object. This objective is achieved by aligning the attention map of SD with the rendered mask of the 3D object. To evaluate the effectiveness of AMA loss in accomplishing this goal, we visualize the attention maps of SD with and without AMA

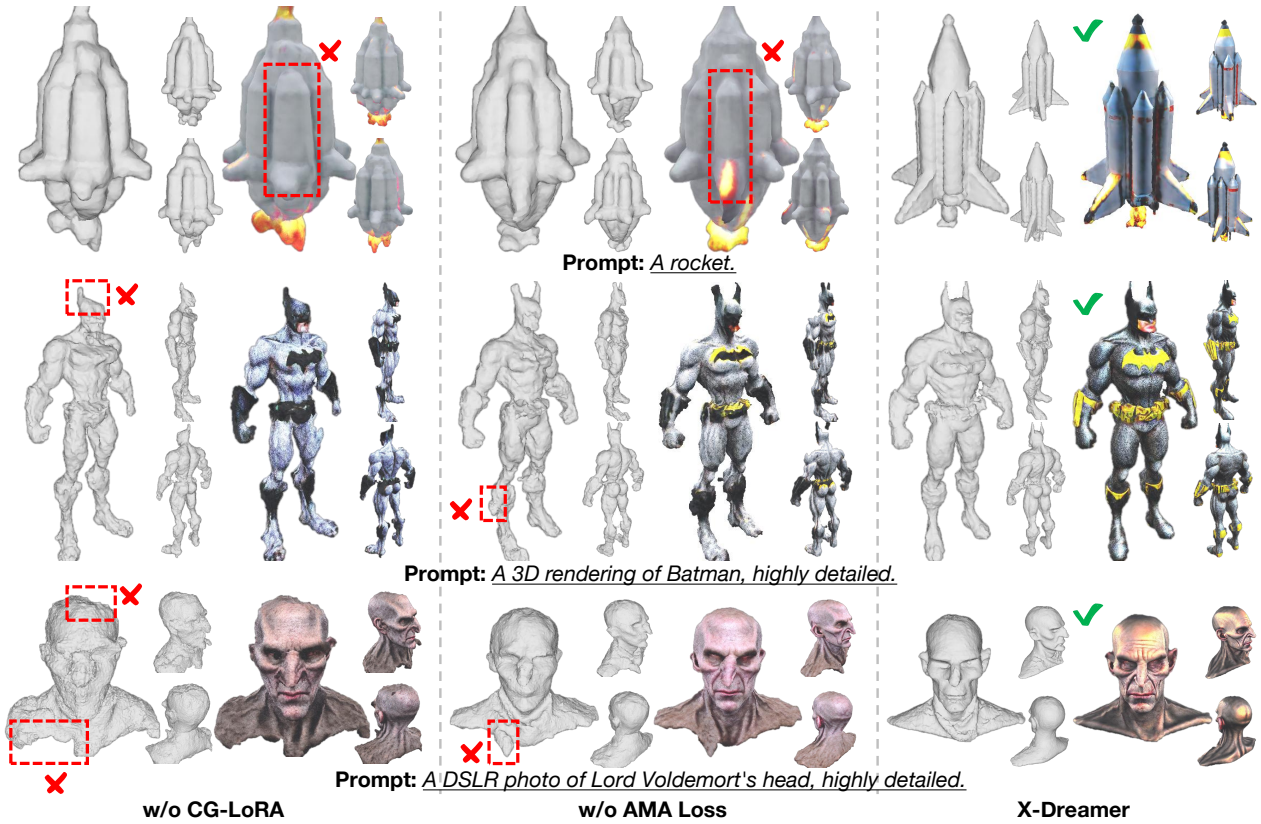
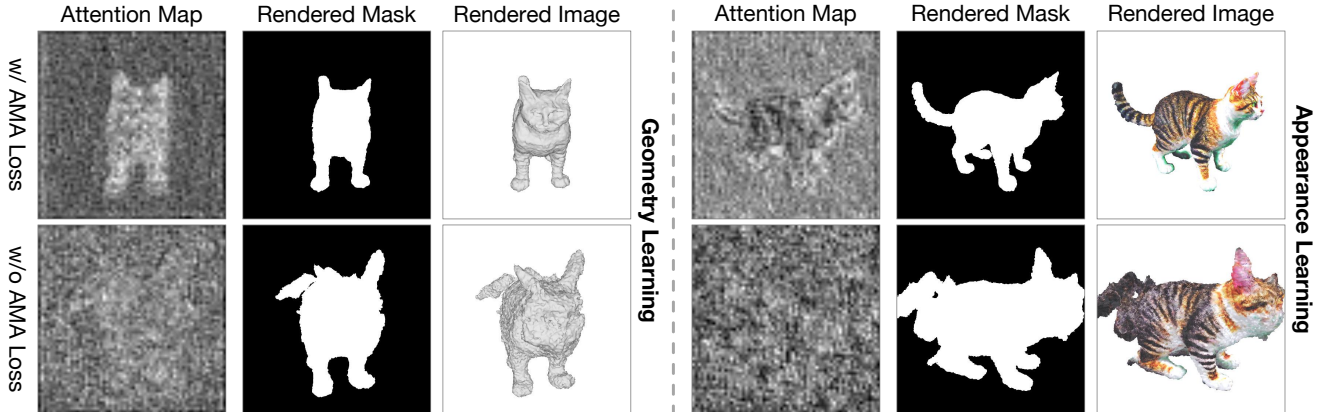


Figure 7. Ablation studies of the proposed X-Dreamer.



Prompt: *A DSLR photo of a cat, highly detailed.*

Figure 8. Visualization of Attention Map, Rendered Mask, and Rendered Image with and without AMA Loss. For clarity, we only visualize the attention map of the first attention layer in SD.

loss at both the geometry learning and appearance learning stages. As depicted in Fig. 8, it can be observed that incorporating AMA loss not only results in improved geometry and appearance of the generated 3D asset, but also concentrates the attention of SD specifically on the foreground object area. The visualizations confirm the efficacy of AMA loss in directing the attention of SD, resulting in improved quality and foreground object focus during geometry and appearance learning stages.

5. Conclusion

This study introduces a groundbreaking framework called X-Dreamer, which is designed to enhance text-to-3D synthesis by addressing the domain gap between text-to-2D and text-to-3D generation. To achieve this, we first propose CG-LoRA, a module that incorporates 3D-associated information, including direction-aware text and camera parameters, into the pretrained Stable Diffusion (SD) model. By doing so, we enable the effective capture of information

relevant to the 3D domain. Furthermore, we design AMA loss to align the attention map generated by SD with the rendered mask of the 3D object. The primary objective of AMA loss is to guide the focus of the text-to-3D model towards the generation of foreground objects. Through extensive experiments, we have thoroughly evaluated the efficacy of our proposed method, which has consistently demonstrated its ability to synthesize high-quality and photorealistic 3D content from given text prompts.

References

- [1] Mohammadreza Armandpour, Huangjie Zheng, Ali Sadeghian, Amir Sadeghian, and Mingyuan Zhou. Reimagine the negative prompt algorithm: Transform 2d diffusion into 3d, alleviate janus problem and beyond. *arXiv preprint arXiv:2304.04968*, 2023. **5, 11**
- [2] Yogesh Balaji, Seungjun Nah, Xun Huang, Arash Vahdat, Jiaming Song, Karsten Kreis, Miika Aittala, Timo Aila, Samuli Laine, Bryan Catanzaro, et al. ediffi: Text-to-image diffusion models with an ensemble of expert denoisers. *arXiv preprint arXiv:2211.01324*, 2022. **1**
- [3] Tom Brown, Benjamin Mann, Nick Ryder, Melanie Subbiah, Jared D Kaplan, Prafulla Dhariwal, Arvind Neelakantan, Pranav Shyam, Girish Sastry, Amanda Askell, et al. Language models are few-shot learners. *Advances in neural information processing systems*, 33:1877–1901, 2020. **3**
- [4] Rui Chen, Yongwei Chen, Ningxin Jiao, and Kui Jia. Fantasia3d: Disentangling geometry and appearance for high-quality text-to-3d content creation. *arXiv preprint arXiv:2303.13873*, 2023. **2, 3, 4, 7, 11**
- [5] Yuan-Chen Guo, Ying-Tian Liu, Ruizhi Shao, Christian Laforte, Vikram Voleti, Guan Luo, Chia-Hao Chen, Zi-Xin Zou, Chen Wang, Yan-Pei Cao, and Song-Hai Zhang. threestudio: A unified framework for 3d content generation. <https://github.com/threestudio-project/threestudio>, 2023. **11**
- [6] Jonathan Ho, Ajay Jain, and Pieter Abbeel. Denoising diffusion probabilistic models. *Advances in neural information processing systems*, 33:6840–6851, 2020. **1**
- [7] Edward J Hu, Yelong Shen, Phillip Wallis, Zeyuan Allen-Zhu, Yuanzhi Li, Shean Wang, Lu Wang, and Weizhu Chen. Lora: Low-rank adaptation of large language models. *arXiv preprint arXiv:2106.09685*, 2021. **3, 5**
- [8] Yukun Huang, Jianan Wang, Ailing Zeng, He Cao, Xianbiao Qi, Yukai Shi, Zheng-Jun Zha, and Lei Zhang. Dreamwaltz: Make a scene with complex 3d animatable avatars. *arXiv preprint arXiv:2305.12529*, 2023. **3**
- [9] Ajay Jain, Ben Mildenhall, Jonathan T Barron, Pieter Abbeel, and Ben Poole. Zero-shot text-guided object generation with dream fields. In *Proceedings of the IEEE/CVF Conference on Computer Vision and Pattern Recognition*, pages 867–876, 2022. **2**
- [10] Ruixiang Jiang, Can Wang, Jingbo Zhang, Menglei Chai, Mingming He, Dongdong Chen, and Jing Liao. Avatarcraft: Transforming text into neural human avatars with parameterized shape and pose control. *arXiv preprint arXiv:2303.17606*, 2023. **3**
- [11] Jiabao Lei, Yabin Zhang, Kui Jia, et al. Tango: Text-driven photorealistic and robust 3d stylization via lighting decomposition. *Advances in Neural Information Processing Systems*, 35:30923–30936, 2022. **2**
- [12] Weiyu Li, Rui Chen, Xuelin Chen, and Ping Tan. Sweetdreamer: Aligning geometric priors in 2d diffusion for consistent text-to-3d. *arXiv preprint arXiv:2310.02596*, 2023. **2, 5, 11**
- [13] Chen-Hsuan Lin, Jun Gao, Luming Tang, Towaki Takikawa, Xiaohui Zeng, Xun Huang, Karsten Kreis, Sanja Fidler, Ming-Yu Liu, and Tsung-Yi Lin. Magic3d: High-resolution text-to-3d content creation. In *Proceedings of the IEEE/CVF Conference on Computer Vision and Pattern Recognition*, pages 300–309, 2023. **2, 3, 7, 11**
- [14] Yiwei Ma, Xiaoqing Zhang, Xiaoshuai Sun, Jiayi Ji, Haowei Wang, Guannan Jiang, Weilin Zhuang, and Rongrong Ji. X-mesh: Towards fast and accurate text-driven 3d stylization via dynamic textual guidance. In *Proceedings of the IEEE/CVF International Conference on Computer Vision*, pages 2749–2760, 2023. **2**
- [15] Stephen McAuley, Stephen Hill, Naty Hoffman, Yoshiharu Gotanda, Brian Smits, Brent Burley, and Adam Martinez. Practical physically-based shading in film and game production. In *ACM SIGGRAPH 2012 Courses*, pages 1–7. 2012. **4**
- [16] Gal Metzer, Elad Richardson, Or Patashnik, Raja Giryes, and Daniel Cohen-Or. Latent-nerf for shape-guided generation of 3d shapes and textures. In *Proceedings of the IEEE/CVF Conference on Computer Vision and Pattern Recognition*, pages 12663–12673, 2023. **2**
- [17] Oscar Michel, Roi Bar-On, Richard Liu, Sagie Benaim, and Rana Hanocka. Text2mesh: Text-driven neural stylization for meshes. In *Proceedings of the IEEE/CVF Conference on Computer Vision and Pattern Recognition*, pages 13492–13502, 2022. **2**
- [18] Ben Mildenhall, Pratul P Srinivasan, Matthew Tancik, Jonathan T Barron, Ravi Ramamoorthi, and Ren Ng. Nerf: Representing scenes as neural radiance fields for view synthesis. *Communications of the ACM*, 65(1):99–106, 2021. **2**
- [19] Nasir Mohammad Khalid, Tianhao Xie, Eugene Belilovsky, and Tiberiu Popa. Clip-mesh: Generating textured meshes from text using pretrained image-text models. In *SIGGRAPH Asia 2022 conference papers*, pages 1–8, 2022. **2**
- [20] Thomas Müller, Alex Evans, Christoph Schied, and Alexander Keller. Instant neural graphics primitives with a multiresolution hash encoding. *ACM Transactions on Graphics (ToG)*, 41(4):1–15, 2022. **4**
- [21] Adam Paszke, Sam Gross, Francisco Massa, Adam Lerer, James Bradbury, Gregory Chanan, Trevor Killeen, Zeming Lin, Natalia Gimelshein, Luca Antiga, et al. Pytorch: An imperative style, high-performance deep learning library. *Advances in neural information processing systems*, 32, 2019. **6**
- [22] Ben Poole, Ajay Jain, Jonathan T Barron, and Ben Mildenhall. Dreamfusion: Text-to-3d using 2d diffusion. *arXiv preprint arXiv:2209.14988*, 2022. **1, 2, 3, 4, 7, 11**

- [23] Alec Radford, Jong Wook Kim, Chris Hallacy, Aditya Ramesh, Gabriel Goh, Sandhini Agarwal, Girish Sastry, Amanda Askell, Pamela Mishkin, Jack Clark, et al. Learning transferable visual models from natural language supervision. In *International conference on machine learning*, pages 8748–8763. PMLR, 2021. [2](#)
- [24] Aditya Ramesh, Pratul Dhariwal, Alex Nichol, Casey Chu, and Mark Chen. Hierarchical text-conditional image generation with clip latents. *arXiv preprint arXiv:2204.06125*, 1(2):3, 2022. [1](#)
- [25] Robin Rombach, Andreas Blattmann, Dominik Lorenz, Patrick Esser, and Björn Ommer. High-resolution image synthesis with latent diffusion models. In *Proceedings of the IEEE/CVF conference on computer vision and pattern recognition*, pages 10684–10695, 2022. [2](#), [3](#)
- [26] Chitwan Saharia, William Chan, Saurabh Saxena, Lala Li, Jay Whang, Emily L Denton, Kamyar Ghasemipour, Raphael Gontijo Lopes, Burcu Karagol Ayan, Tim Salimans, et al. Photorealistic text-to-image diffusion models with deep language understanding. *Advances in Neural Information Processing Systems*, 35:36479–36494, 2022. [1](#), [2](#), [3](#)
- [27] Christoph Schuhmann, Romain Beaumont, Richard Vencu, Cade Gordon, Ross Wightman, Mehdi Cherti, Theo Coombes, Aarush Katta, Clayton Mullis, Mitchell Wortsman, et al. Laion-5b: An open large-scale dataset for training next generation image-text models. *Advances in Neural Information Processing Systems*, 35:25278–25294, 2022. [1](#)
- [28] Junyoung Seo, Wooseok Jang, Min-Seop Kwak, Jaehoon Ko, Hyeonsu Kim, Junho Kim, Jin-Hwa Kim, Jiyoung Lee, and Seungryong Kim. Let 2d diffusion model know 3d-consistency for robust text-to-3d generation. *arXiv preprint arXiv:2303.07937*, 2023. [3](#)
- [29] Tianchang Shen, Jun Gao, Kangxue Yin, Ming-Yu Liu, and Sanja Fidler. Deep marching tetrahedra: a hybrid representation for high-resolution 3d shape synthesis. *Advances in Neural Information Processing Systems*, 34:6087–6101, 2021. [4](#)
- [30] Jascha Sohl-Dickstein, Eric Weiss, Niru Maheswaranathan, and Surya Ganguli. Deep unsupervised learning using nonequilibrium thermodynamics. In *International conference on machine learning*, pages 2256–2265. PMLR, 2015. [1](#)
- [31] Yang Song, Jascha Sohl-Dickstein, Diederik P Kingma, Abhishek Kumar, Stefano Ermon, and Ben Poole. Score-based generative modeling through stochastic differential equations. *arXiv preprint arXiv:2011.13456*, 2020. [1](#)
- [32] Junshu Tang, Tengfei Wang, Bo Zhang, Ting Zhang, Ran Yi, Lizhuang Ma, and Dong Chen. Make-it-3d: High-fidelity 3d creation from a single image with diffusion prior. *arXiv preprint arXiv:2303.14184*, 2023. [3](#)
- [33] Kenneth E Torrance and Ephraim M Sparrow. Theory for off-specular reflection from roughened surfaces. *Josa*, 57(9):1105–1114, 1967. [4](#)
- [34] Patrick von Platen, Suraj Patil, Anton Lozhkov, Pedro Cuenca, Nathan Lambert, Kashif Rasul, Mishig Davaadorj, and Thomas Wolf. Diffusers: State-of-the-art diffusion models. <https://github.com/huggingface/diffusers>, 2022. [6](#)
- [35] Haochen Wang, Xiaodan Du, Jiahao Li, Raymond A Yeh, and Greg Shakhnarovich. Score jacobian chaining: Lifting pretrained 2d diffusion models for 3d generation. In *Proceedings of the IEEE/CVF Conference on Computer Vision and Pattern Recognition*, pages 12619–12629, 2023. [2](#)
- [36] Zhengyi Wang, Cheng Lu, Yikai Wang, Fan Bao, Chongxuan Li, Hang Su, and Jun Zhu. Prolificdreamer: High-fidelity and diverse text-to-3d generation with variational score distillation. *arXiv preprint arXiv:2305.16213*, 2023. [2](#), [3](#), [7](#), [11](#)
- [37] Jiacheng Wei, Hao Wang, Jiashi Feng, Guosheng Lin, and Kim-Hui Yap. Taps3d: Text-guided 3d textured shape generation from pseudo supervision. In *Proceedings of the IEEE/CVF Conference on Computer Vision and Pattern Recognition*, pages 16805–16815, 2023. [2](#)
- [38] Lvmin Zhang, Anyi Rao, and Maneesh Agrawala. Adding conditional control to text-to-image diffusion models. In *Proceedings of the IEEE/CVF International Conference on Computer Vision*, pages 3836–3847, 2023. [3](#)

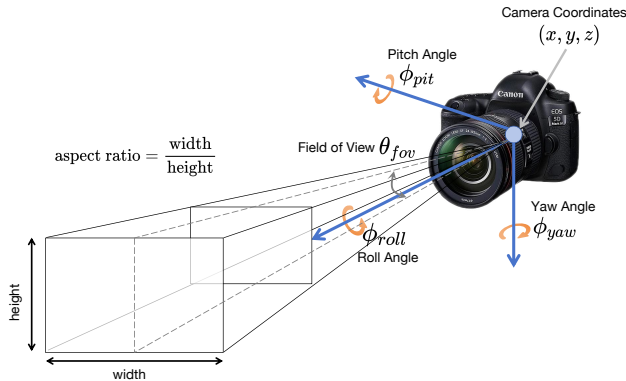


Figure 9. Illustration of camera parameters.

6. Appendix

6.1. Camera Parameters

In this section, we present a comprehensive elucidation of the camera parameters discussed in our paper, namely $C = \{x, y, z, \phi_{yaw}, \phi_{pit}, \phi_{roll}, \theta_{fov}\}$. These parameters play a fundamental role in our research and are crucial for understanding the underlying principles of our methodology. Fig. 9 visually depicts the camera parameters in relation to our work. The variables x , y , and z correspond to the camera’s coordinates within the world coordinate system, providing spatial information about its positioning. The rotation angles ϕ_{yaw} , ϕ_{pit} , and ϕ_{roll} describe the camera’s orientation along the x , y , and z axes, respectively. By controlling these angles, we ensure that objects depicted in the rendered images maintain their desired orientation. Specifically, to achieve a stable rendering process, we set ϕ_{roll} to a constant value of 0° throughout the training phase. Another critical parameter is θ_{fov} , which denotes the camera’s field of view. This parameter determines the angular range captured in the rendered image. Moreover, we also consider the aspect ratio, representing the proportional relationship between the width and height of the rendered area. In our implementation, we set the aspect ratio to 1, ensuring a balanced rendering output.

6.2. More Visualization

In this section, we present a comprehensive set of generated results that offer compelling evidence to substantiate the exceptional capabilities of our proposed X-Dreamer in producing robust and top-tier 3D assets. The additional visualization results, available in Fig. 10, Fig. 11, Fig. 12, Fig. 13, and Fig. 14, not only serve to validate the effectiveness of our approach but also emphasize its significant potential for various applications in the field. These results are pivotal in establishing the credibility and superiority of our approach, bolstering the confidence in its practicality and effectiveness.

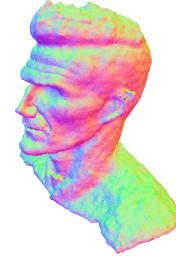
6.3. More Comparison

In this section, we present an extensive visualization comparison between our proposed X-Dreamer and four prominent baselines in the field, namely DreamFusion [22], Magic3D [13], Fantasia3D [4], and ProlificDreamer [36]. By incorporating these baselines into our analysis, we aim to provide a comprehensive assessment of the efficacy and superiority of our method. Since the codes of some methods [13, 22, 36] have not been publicly available, we present the results obtained by implementing these methods in threestudio [5]. As depicted in Fig. 17, our observations reveal a striking disparity between the generated results of X-Dreamer and those of the baselines. Notably, the outputs produced by our proposed X-Dreamer exhibit a significantly higher degree of realism, unmistakably highlighting the unparalleled effectiveness of our methodology. This stark contrast serves as a compelling visual testament to the exceptional quality and fidelity achieved by our approach. In Fig. 18, we present a comprehensive comparison of our methods with four baselines, using the images provided in their original papers. Our results clearly demonstrate the superiority of our proposed X-Dreamer in terms of realism and optimization time compared to DreamFusion [22], Magic3D [13], and Fantasia3D [4]. When compared to ProlificDreamer [36], our X-Dreamer achieves comparable results. It is worth noting that the learning process for geometry and appearance in X-Dreamer takes only approximately 27 minutes, whereas ProlificDreamer requires over 8 hours.

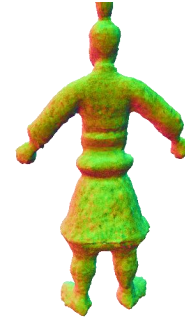
The remarkable realism attained by X-Dreamer can be partly attributed to the incorporation of our novel CG-LoRA technique, which seamlessly integrates camera information into the text-to-3D model. By leveraging this innovative strategy, X-Dreamer ensures the generation of objects with consistent perspectives, thereby eliminating the prevalent issue of inconsistent perspectives, commonly known as the Janus Problem [1, 12], encountered by other baselines. This significant advantage further consolidates the superiority of X-Dreamer over its competitors. Furthermore, our proposed AMA loss plays also a pivotal role in enhancing the generation process. By emphasizing the foreground object through the AMA loss, X-Dreamer effectively allocates more attention to crucial details, resulting in the generation of photorealistic 3D objects with exceptional geometry and appearance intricacies. This attention to detail sets X-Dreamer apart from other baselines, revealing its capacity to produce outputs that surpass existing methods in terms of fidelity and visual appeal. By incorporating camera information through CG-LoRA and leveraging the AMA loss to enhance foreground object generation, X-Dreamer establishes itself as a cutting-edge solution capable of generating photorealistic 3D objects with superior geometry and appearance details. These findings substantiate the efficacy and practical relevance of our methodology, thus contribut-



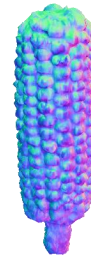
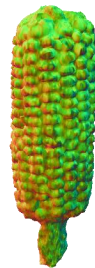
A marble bust of an angel, 3D model, high resolution.



A DSLR photo of David Beckham's head, highly detailed, 8K, HD.



A DSLR photo of the Terracotta Army, 3D model, high resolution.



A DSLR photo of a corn, highly detailed, 8K, HD.

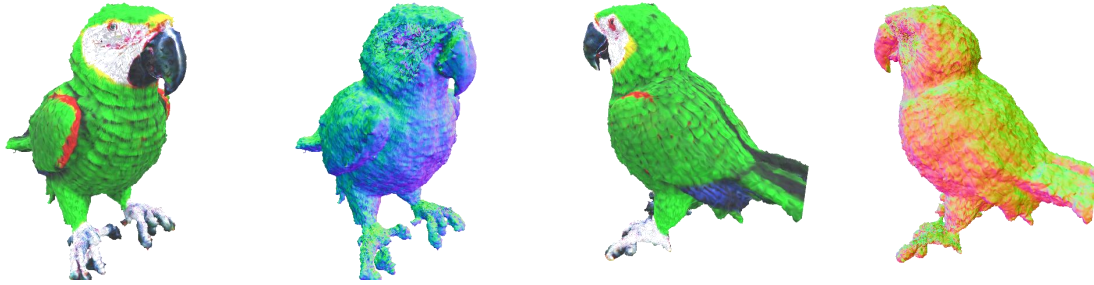
Figure 10. More text-to-3D generation results of the proposed X-Dreamer.

ing to the advancement of the field and reinforcing the vital role of X-Dreamer in pushing the boundaries of 3D object generation.

6.4. Three PBR Material Terms

The Three PBR Material Terms in Physically Based Rendering (PBR) play a crucial role in describing material appearance and behavior. Firstly, the Diffuse Term $k_d \in \mathbb{R}^3$

accurately represents how the material responds to diffuse lighting. This term is captured by a three-dimensional vector that denotes the material's diffuse color. Secondly, the Roughness and Metallic Term $k_{rm} \in \mathbb{R}^2$ effectively captures the material's roughness and metallic properties. It is represented by a two-dimensional vector that conveys the values of roughness and metallicness. Roughness quantifies the surface smoothness, while metallicness indicates



A parrot, 3d model, highly detailed, 8K, HD.



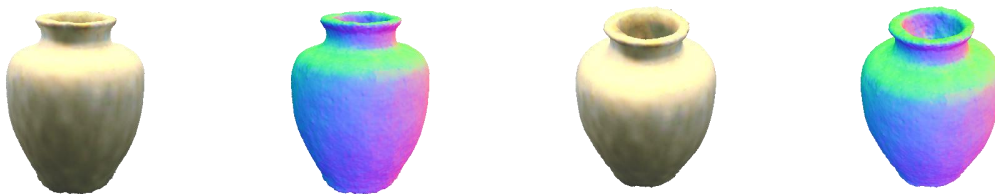
A DSLR photo of a macaron, 8K, HD, high resolution.



A DSLR photo of a pear, highly detailed, 8K, HD.



A DSLR photo of a red apple, highly detailed.



A DSLR photo of a vase, highly detailed, 8K, HD.

Figure 11. More text-to-3D generation results of the proposed X-Dreamer.

the presence of metallic properties in the material. These terms collectively contribute to the overall visual realism

of the rendered scene. Additionally, the Normal Variation Term $k_n \in \mathbb{R}^3$ plays a crucial role in characterizing varia-

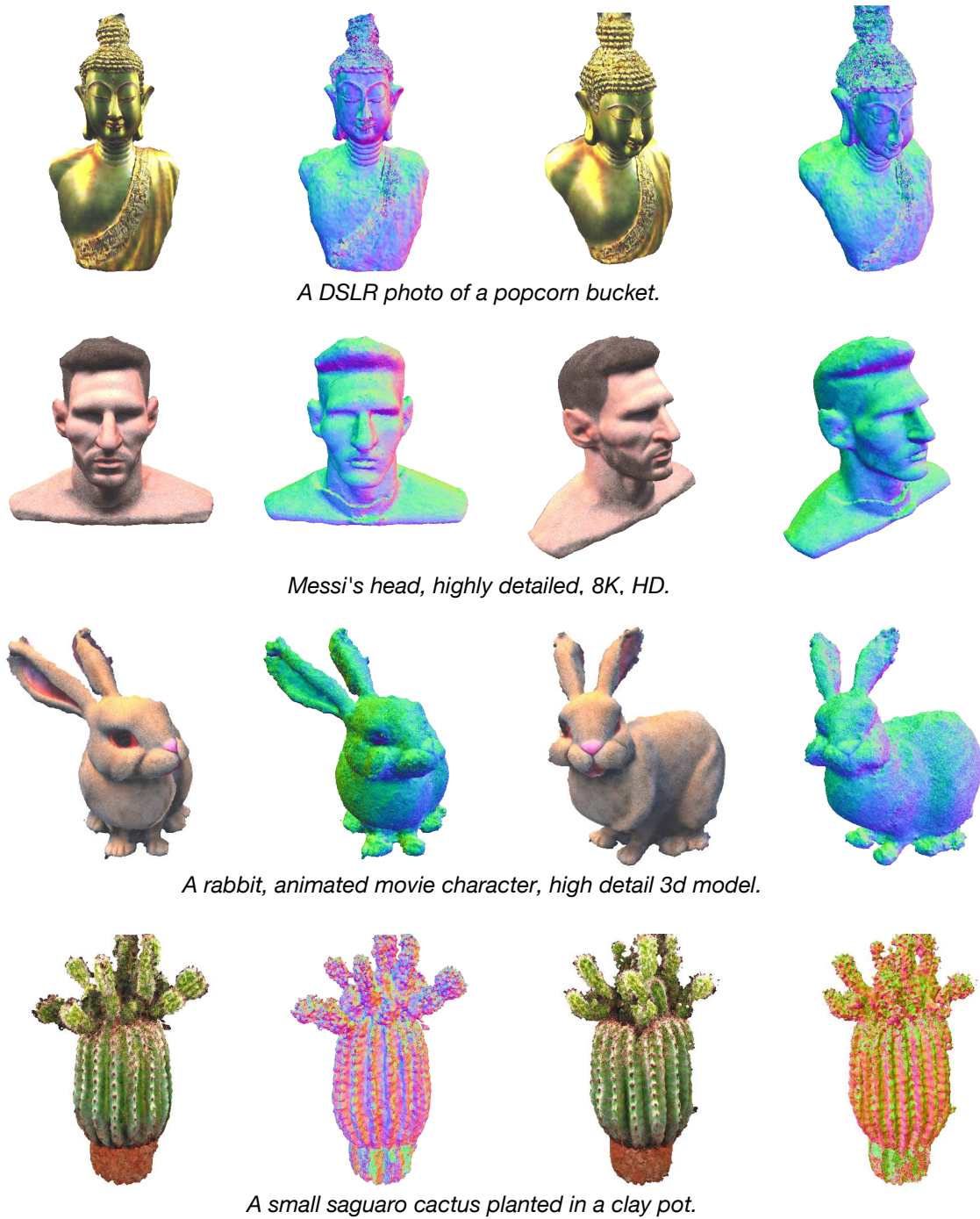


Figure 12. More text-to-3D generation results of the proposed X-Dreamer.

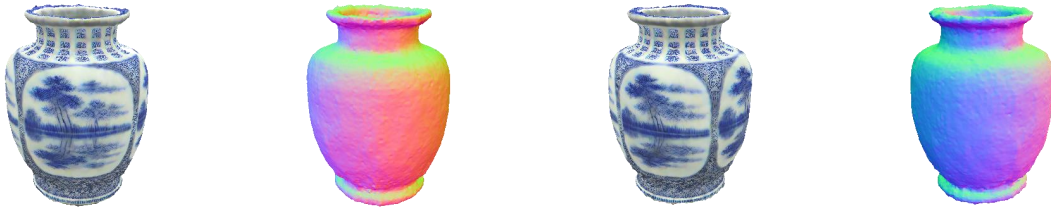
tions in surface normals. This term, typically used in conjunction with a normal map, enables the simulation of fine details and textures on the material's surface. During the rendering process, these three PBR material terms interact to accurately simulate the optical properties exhibited by

real-world materials. This integration facilitates rendering engines in achieving high-quality rendering results and generating realistic virtual scenes.

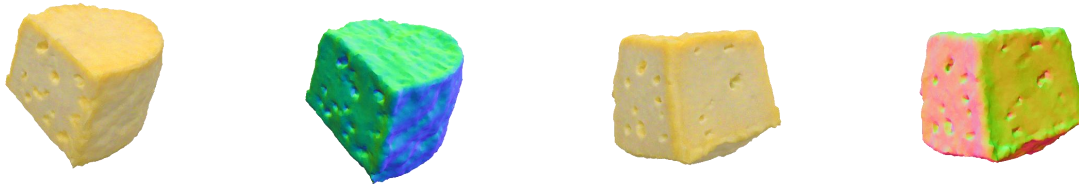
To demonstrate the effectiveness of these material terms, we present visualizations in Fig. 19. The generated re-



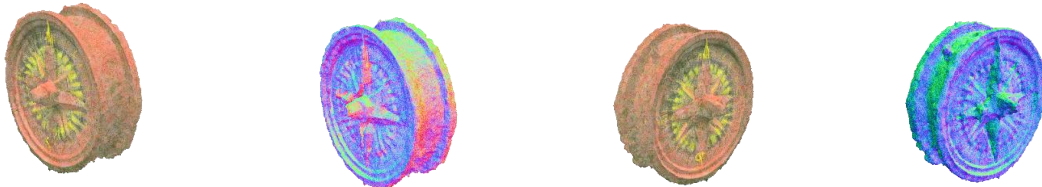
A DSLR photo of a popcorn bucket.



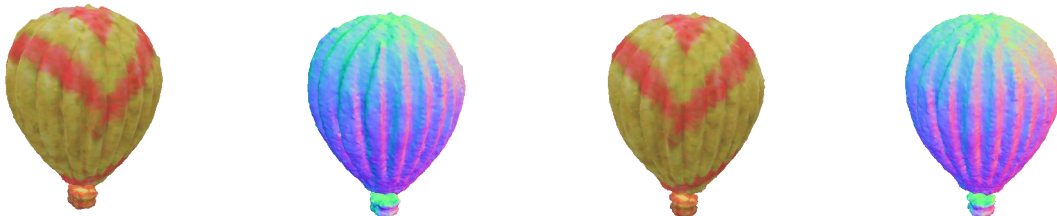
A DSLR photo of a blue and white porcelain vase, highly detailed, 8K, HD.



A DSLR photo of cheese, high resolution.



A DSLR photo of a compass, highly detailed, 8K, HD.

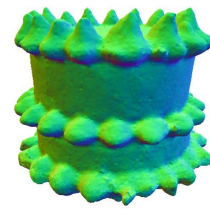
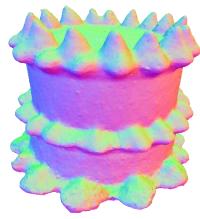


A DSLR photo of hot air balloon, highly detailed, 8K, HD, 3D model.

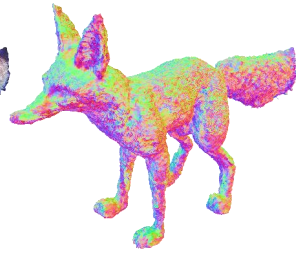
Figure 13. More text-to-3D generation results of the proposed X-Dreamer.

sults using X-Dreamer showcase accurate representations for each of the three material terms. When combined, these terms collectively contribute to the creation of a realistic rendering. In particular, the visualization of the Diffuse Term $k_d \in \mathbb{R}^3$ exhibits similarities to the rendered im-

age in certain cases. However, the rendered image displays a higher level of detail compared to the Diffuse Term $k_d \in \mathbb{R}^3$. Zooming in on the images, as shown in the last row of Fig. 19 reveals that the rendered image accurately depicts the details of stomata generated during the bread



A birthday cake, 3D model, highly detailed.



A DSLR photo of a fox, highly detailed.



A DSLR photo of a lotus, highly detailed, 8K, HD.



A DSLR photo of red rose, highly detailed, 8K, HD.



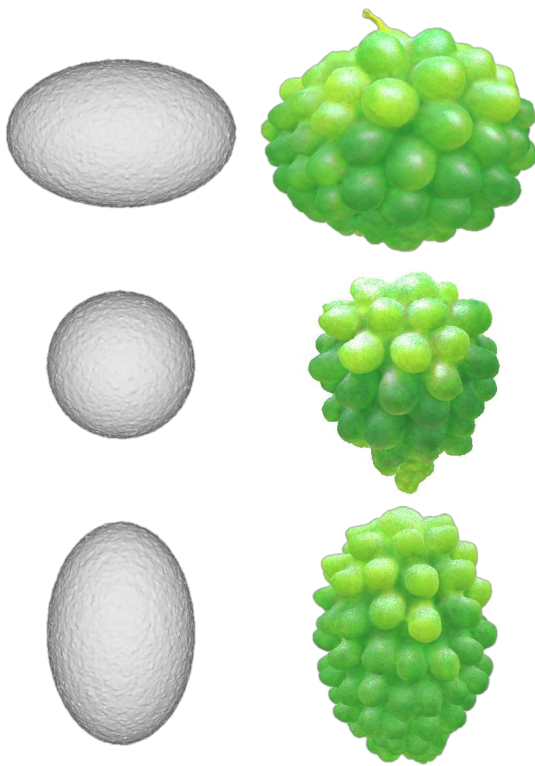
A stack of pancakes covered in maple syrup.

Figure 14. More text-to-3D generation results of the proposed X-Dreamer.

fermentation process. In contrast, the stomata details in the Diffuse Term $k_d \in \mathbb{R}^3$ appear blurry. Thus, it is evident that these three material terms play a crucial role in generating realistic photos, as they collectively contribute to the

accurate representation of material properties and the fine details observed in the rendered images.

Initialization Shape **Text-to-3D Result**



Prompt: Green grapes, highly detailed, 8K, HD.

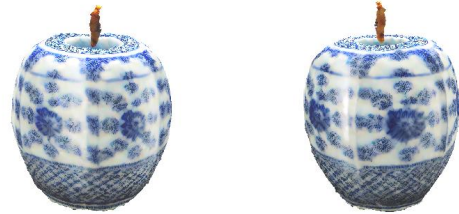
Figure 15. Text-to-3D results using the same textual prompt with different initialization ellipsoids.

6.5. Ablation Study of CG-LoRA

In our implementation, the parameters of CG-LoRA are dynamically generated based on two key factors related to camera information: camera parameters and direction-aware text. To thoroughly investigate the impact of these camera information terms on X-Dreamer, we conducted ablation experiments, dynamically generating CG-LoRA parameters based solely on one of these terms. The results, as illustrated in Fig. 20, clearly demonstrate that when using only one type of camera information term, the geometry and appearance quality of the generated results are significantly diminished compared to those produced by X-Dreamer. For example, as shown in the third row of Fig. 20, when utilizing the CG-LoRA solely related to direction-aware text, the geometry quality of the generated cookies appears poor. Similarly, as depicted in the last row of Fig. 20, employing the CG-LoRA solely based on camera parameters results in diminished geometry and appearance quality for the pumpkin. These findings highlight the importance of both camera parameters and direction-aware text in generating



A sliced loaf of fresh bread and a cabbage.



A DSLR photo of a blue and white porcelain vase and an apple, highly detailed, 8K, HD.

Figure 16. Limitations of X-Dreamer.

high-quality 3D assets. The successful generation of parameters for CG-LoRA relies on the synergy between these two camera information terms, emphasizing their crucial role in achieving superior geometry and appearance in the generated assets.

6.6. Attention Map Visualization w/ and w/o the Proposed Modules

To gain insights into the effectiveness of the proposed modules on the attention map, we conducted visualizations of the attention map of X-Dreamer without CG-LoRA and AMA loss, as depicted in Fig. 21 and Fig. 22, respectively. Our observations reveal that both proposed modules effectively guide X-Dreamer to focus on the foreground object, enhancing its attention capabilities. In particular, Fig. 21 and Fig. 22 showcase the attention maps of X-Dreamer during the geometry learning stage and the appearance learning stage, respectively. From Fig. 21, it is evident that removing either CG-LoRA or AMA loss from X-Dreamer results in less-targeted attention maps. This outcome aligns with our expectations, as the AMA loss directly aligns the attention map with the rendered mask, enabling the model to concentrate on the foreground objects. An intriguing finding is that CG-LoRA also facilitates the model’s ability to focus on foreground objects. This can be attributed to the incorporation of camera information in X-Dreamer through CG-LoRA, which enhances the model’s perception of the position and shape of foreground objects. Consequently,



Figure 17. More comparison with State-of-the-Art (SOTA) methods.

more accurate attention maps are generated. Similar observations can be made during the appearance modeling stage, as depicted in Fig. 22. The attention maps generated by X-Dreamer without CG-LoRA or AMA loss demonstrate a

reduced focus on the foreground object. These findings provide strong evidence for the effectiveness of the proposed modules in guiding X-Dreamer to attend to the foreground objects accurately. The inclusion of camera information

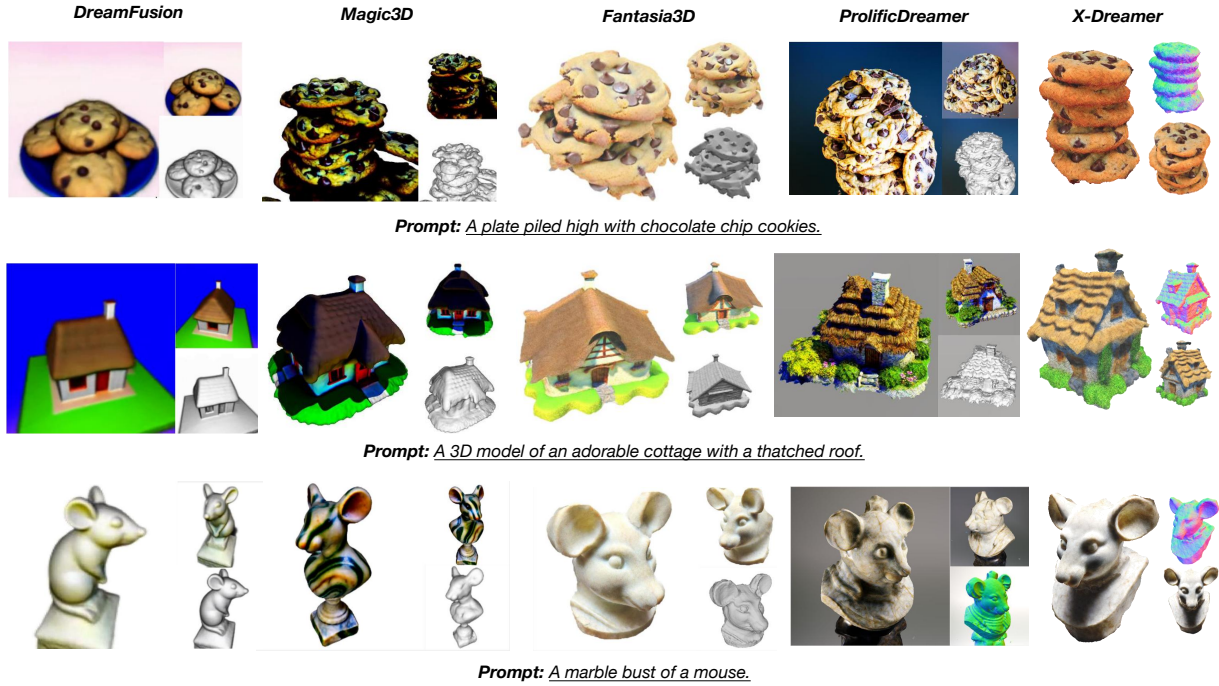


Figure 18. More comparison with State-of-the-Art (SOTA) methods.

through CG-LoRA proves to be a valuable addition, enabling the model to generate attention maps that align with the desired foreground objects throughout the geometry and appearance modeling stages.

6.7. Different Initialization Ellipsoids

In this section, our objective is to investigate the impact of varying initialization ellipsoids under the same textual prompt. As illustrated in Fig. 15, when we refrain from specifying a particular shape in the text prompt and opt for initialization using ellipsoids of diverse shapes, the outcomes of text-to-3D transformation demonstrate a notable compatibility with mesh-related initialization procedures. This observation is inherently logical. When the model undergoes optimization based on a given mesh, it promptly acquires a local optimal solution and tends to oscillate within its proximity during the optimization process. This behavior makes it inherently challenging for the model to escape this limited range and explore alternative local optimal solutions.

6.8. Rendered Images under Different Environment Maps

Our method, while employing a fixed environment for training the model, offers significant advantages and flexibility in the rendering of 3D assets generated by X-Dreamer. It is worth noting that these assets are not limited to a single

environment; instead, they possess the capability to be rendered in diverse environments, expanding their applicability and adaptability. The visual evidence presented in Fig. 23 and Fig. 24 reinforces our claim. By utilizing different environment maps, we can readily observe the striking variations in the appearance of the rendered images of these 3D assets. This compelling demonstration showcases the inherent versatility and potential of X-Dreamer’s generated assets to seamlessly integrate into various rendering engines. The ability to effectively address the challenges posed by different lighting conditions is a crucial aspect of any rendering engine. By leveraging the capabilities of X-Dreamer, we unlock the possibility of using its 3D assets in a multitude of rendering engines. This versatility ensures that the assets can adapt and thrive in diverse lighting scenarios, enabling them to meet the demands of real-world applications in fields such as architecture, virtual reality, and computer graphics.

6.9. Limitation

One limitation of the proposed X-Dreamer is its inability to generate multiple objects simultaneously. When the input text prompt contains two distinct objects, X-Dreamer may produce a mixed object that combines properties of both objects. A clearer understanding of this limitation can be gained by referring to Fig. 16. In the first row of Fig. 16, our intention is for X-Dreamer to generate “A sliced loaf of

Rendered Image

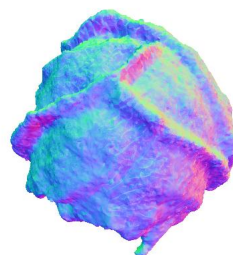
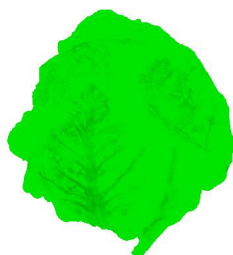
k_d

k_{rm}

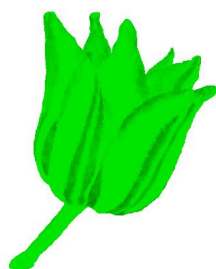
k_n



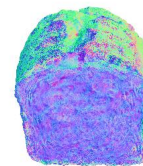
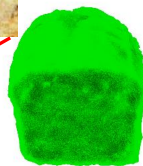
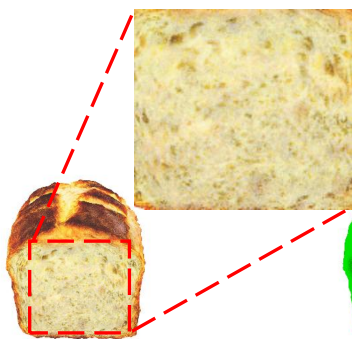
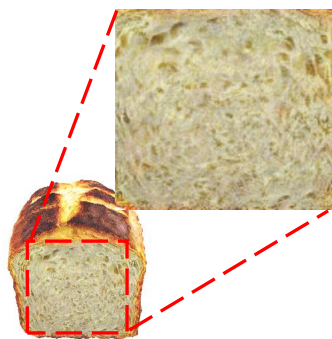
A plate piled high with chocolate chip cookies.



A cabbage, highly detailed.



A blue tulip.



A sliced loaf of fresh bread.

Figure 19. Visualization of Three Material Terms.

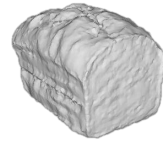
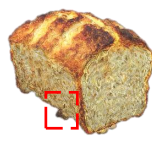
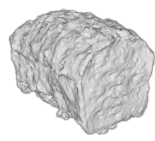
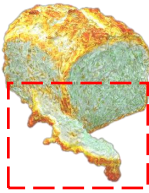
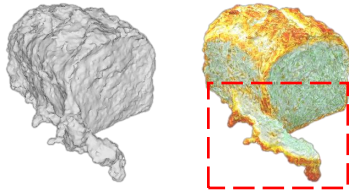
fresh bread and a cabbage.” However, the resulting output consists of a bread with a few cabbage leaves, indicating the

model’s difficulty in generating separate objects accurately. Similarly, in the second row of Fig. 16, we aim to generate

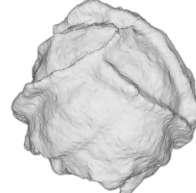
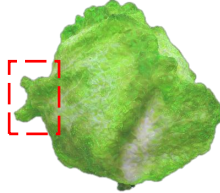
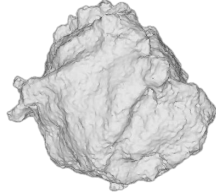
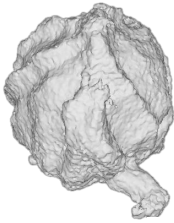
**W/ CG-LoRA
(camera parameters)**

**W/ CG-LoRA
(direction-aware text)**

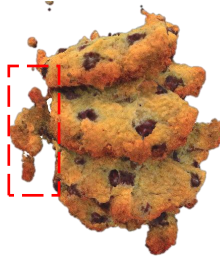
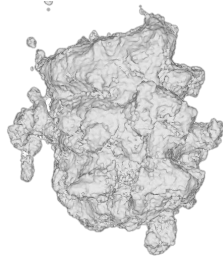
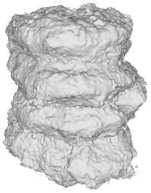
W/ CG-LoRA



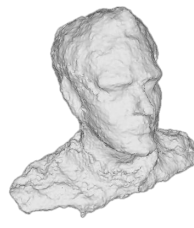
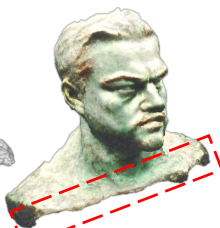
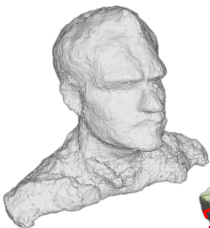
A sliced loaf of fresh bread.



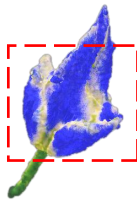
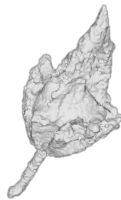
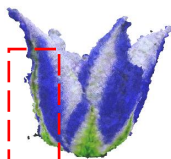
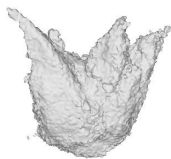
A cabbage, highly detailed.



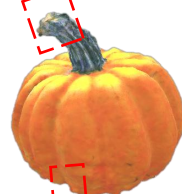
A plate piled high with chocolate chip cookies.



A statue of Leonardo DiCaprio's head.



A blue tulip.



A pumpkin, highly detailed, 8K, HD.

Figure 20. Ablation Study of CG-LoRA.

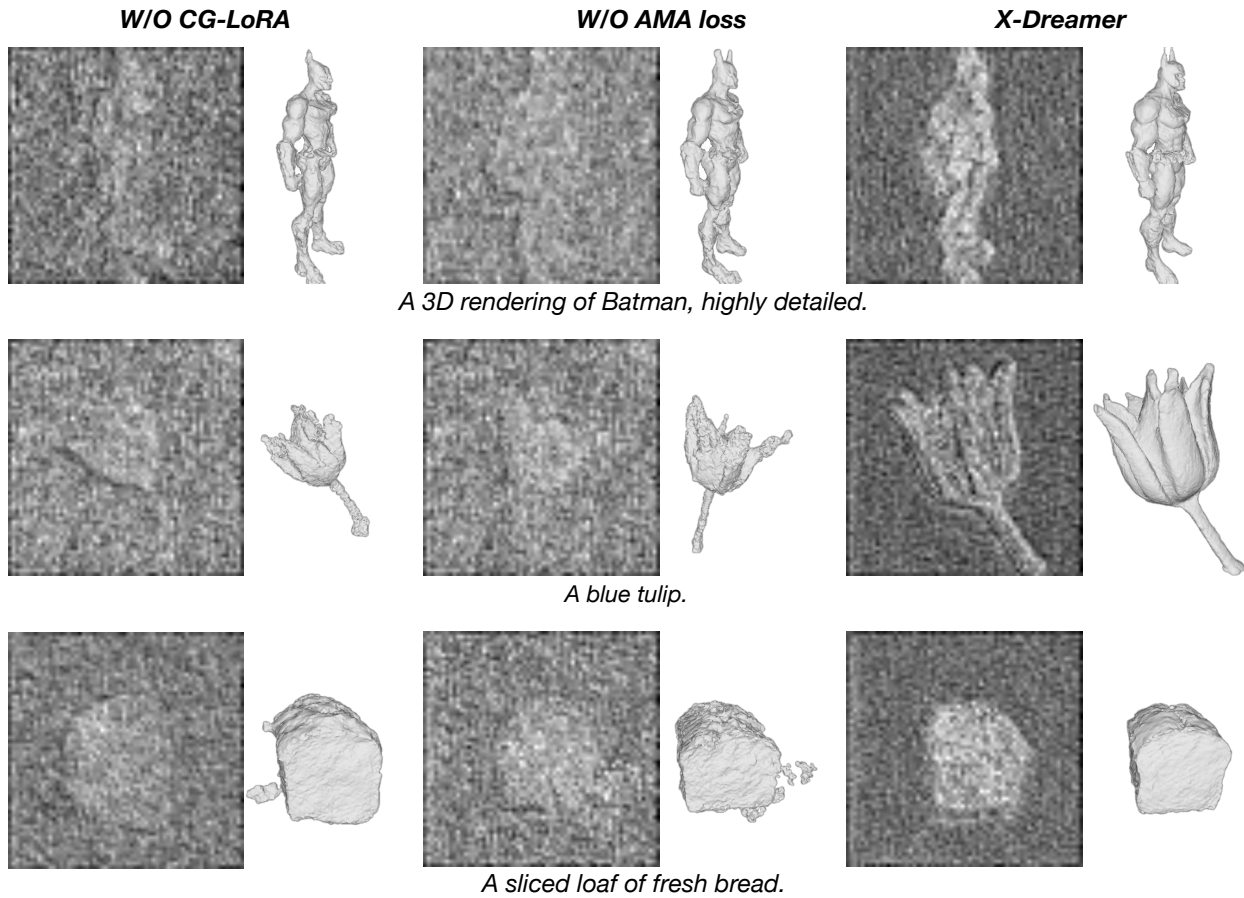


Figure 21. Attention map comparisons w/ and w/o the proposed modules for geometry learning.

“A blue and white porcelain vase and an apple.” However, the output depicts a blue and white porcelain vase with a shape resembling an apple. Nevertheless, it is important to note that this limitation does not significantly undermine the value of our work. In applications such as games and movies, each object functions as an independent entity, capable of creating complex scenes through interaction with other objects. Our primary objective is to generate high-quality 3D objects, and while the current limitation exists, it does not diminish the overall quality and utility of our approach.

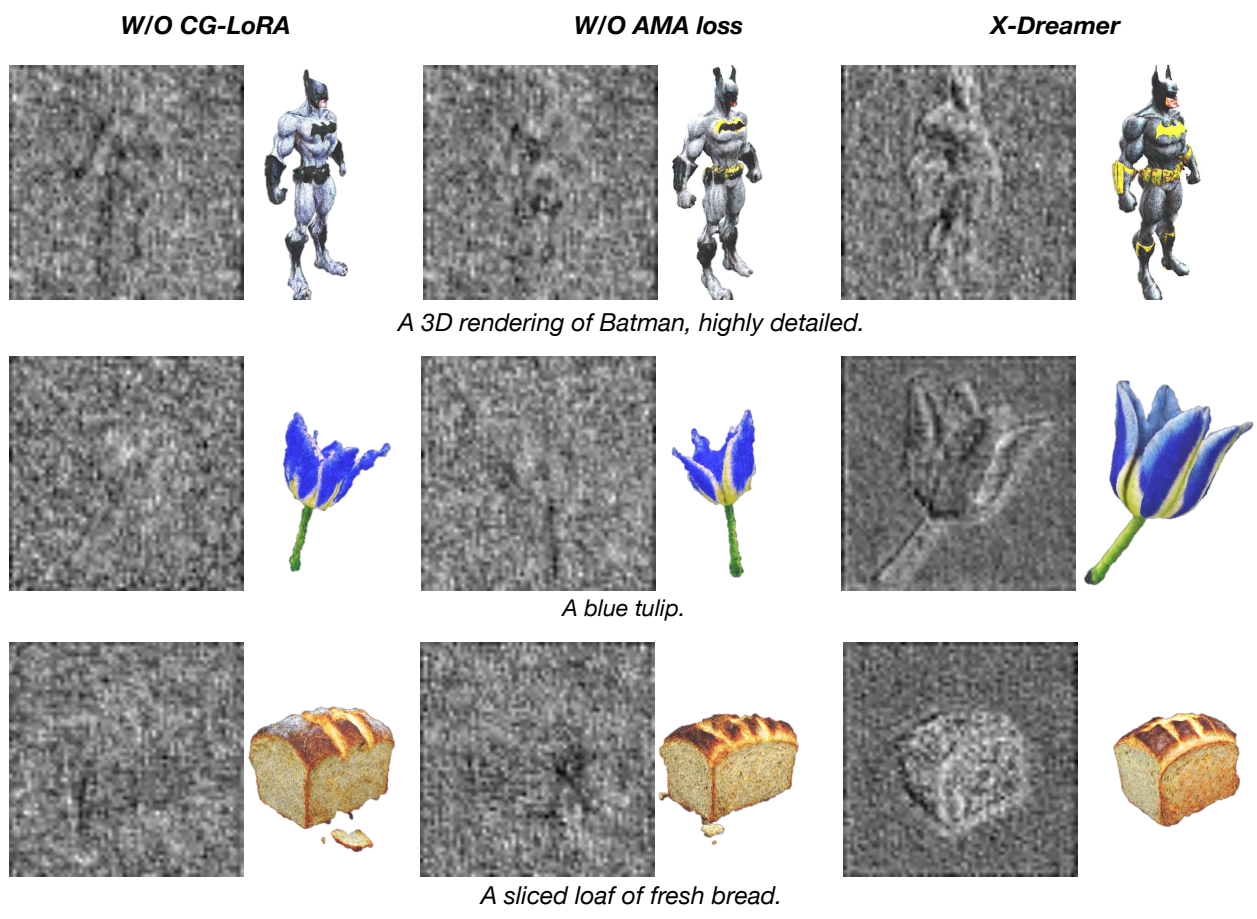


Figure 22. Attention map comparisons w/ and w/o the proposed modules for appearance learning.



A statue of Leonardo DiCaprio's head.



A plate piled high with chocolate chip cookies.



A 3D rendering of Batman, highly detailed.



A pumpkin, highly detailed,8K,HD.



A beautifully carved wooden queen chess piece.

Environment Map



Figure 23. Rendered images of generated 3D assets under different environment maps.

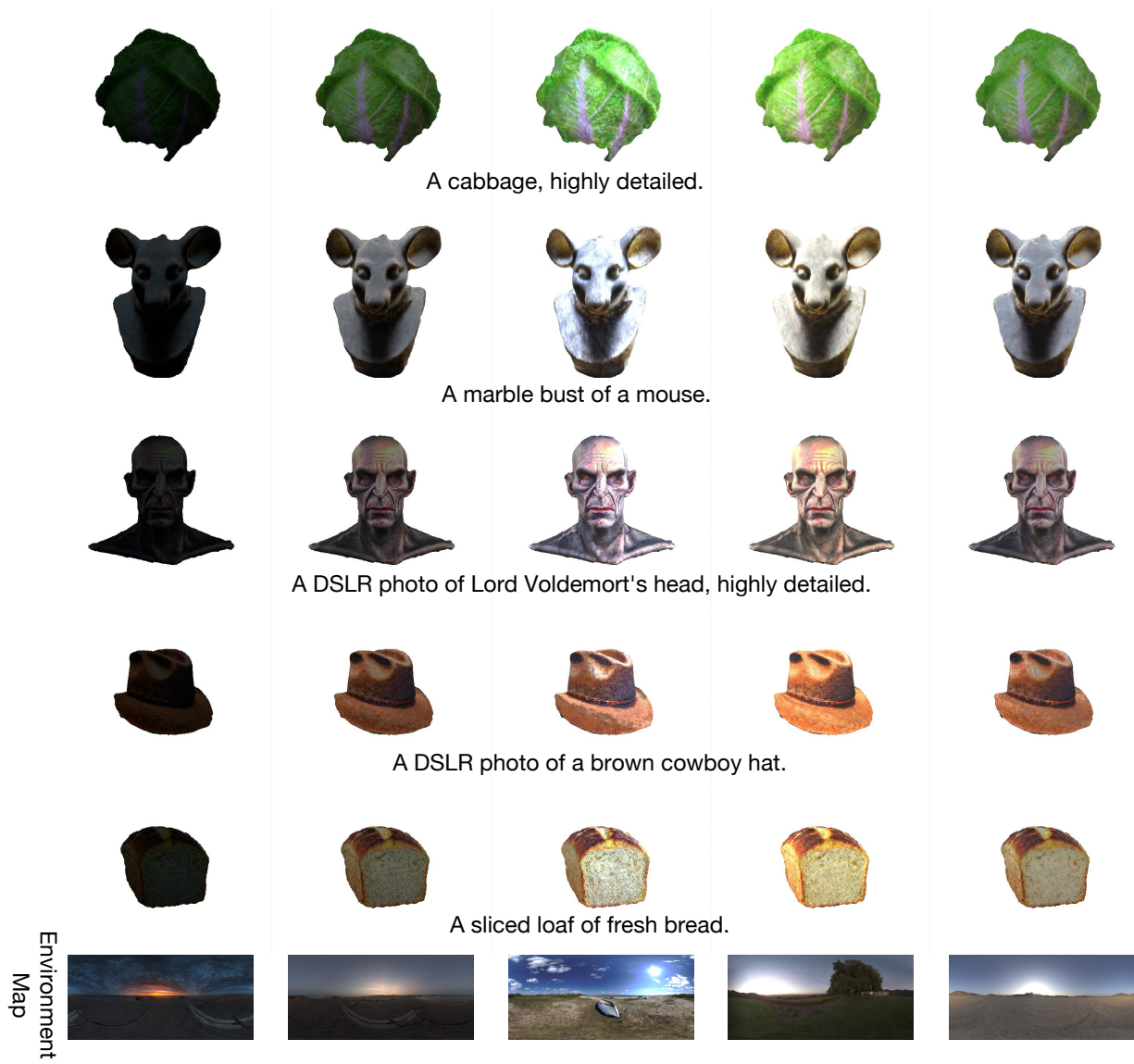


Figure 24. Rendered images of generated 3D assets under different environment maps.